C Journal of Carbon Research

MDPI

Article

Expanded Graphite (EG) Stabilization of Stearic and Palmitic Acid Mixture for Thermal Management of Photovoltaic Cells

Sereno Sacchet [1,*], Francesco Valentini [1], Alice Benin [2], Marco Guidolin [2], Riccardo Po [3] and Luca Fambri [1,*]

[1] Department of Industrial Engineering and INSTM Research Unit, University of Trento, Via Sommarive 9 38123 Trento, Italy; francesco.valentini@unitn.it
[2] New Energies, Renewable Energies and Materials Science Research Center, Eni S.p.A., 30175 Marghera, Italy; alice.benin@eni.com (A.B.); marco.guidolin@eni.com (M.G.)
[3] New Energies, Renewable Energies and Materials Science Research Center, "Istituto Guido Donegani", Eni S.p.A., 28100 Novara, Italy; riccardo.po@eni.com
* Correspondence: sereno.sacchet@unitn.it (S.S.); luca.fambri@unitn.it (L.F.); Tel.: +39-0461-282413 (L.F.)

Citation: Sacchet, S.; Valentini, F.; Benin, A.; Guidolin, M.; Po, R.; Fambri, L. Expanded Graphite (EG) Stabilization of Stearic and Palmitic Acid Mixture for Thermal Management of Photovoltaic Cells. *C* **2024**, *10*, 46. https://doi.org/10.3390/c10020046

Academic Editor: Gil Goncalves

Received: 15 March 2024
Revised: 2 May 2024
Accepted: 10 May 2024
Published: 15 May 2024

Copyright: © 2024 by the authors. Licensee MDPI, Basel, Switzerland. This article is an open access article distributed under the terms and conditions of the Creative Commons Attribution (CC BY) license (https://creativecommons.org/licenses/by/4.0/).

Supplementary Materials

1. Pressed expanded graphite (EG) pellets

The skeleton density of the expanded graphite (EG) was evaluated performing 99 measurements through Anton PAAR Ultrapyc 5000 helium pycnometer for comparison with graphite theoretical density (2.26 g/cm^3) due to the open nature of the porosity. In order to occupy enough volume of the chamber, having volume of 4.5 cm^3, the EG powder was cold compacted obtaining two disks having diameter of 13 mm (Figure S1). The obtained density was 2.268 ± 0.004 g/cm^3, perfectly matching the theoretical value.

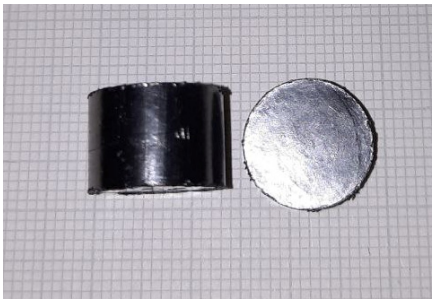

Figure S1. Pressed EG disks of 13.0 mm of diameter for the evaluation of density. On the left density 1.87 g/cm3 (2.274 g, thickness 9.16 mm), on the right density 1.90 g/cm^3 (0.823 g and 3.27 mm thickness).

The disk of thickness 3.27 mm was then used for the determination of the thermal conductivity with laser flash analysis (LFA).

2. Thermal gravimetric analysis (TGA) in air atmospheres

In Figure S2 the TGA curves in air of neat PA-SA, EG and samples investigated as residual mass and derivative of weight loss (DTGA) are reported, while in Table S1 the characteristic temperatures and weight fractions are listed.

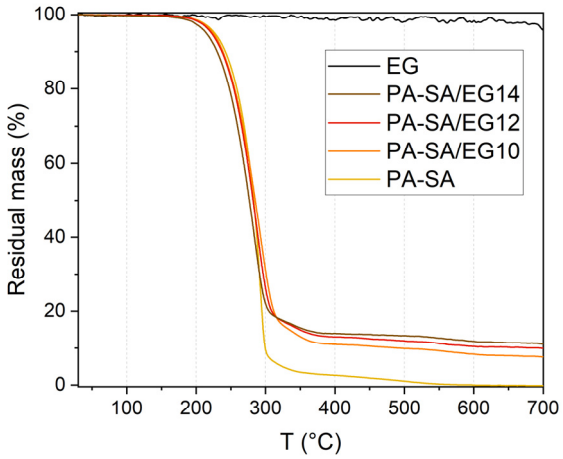

(**a**)

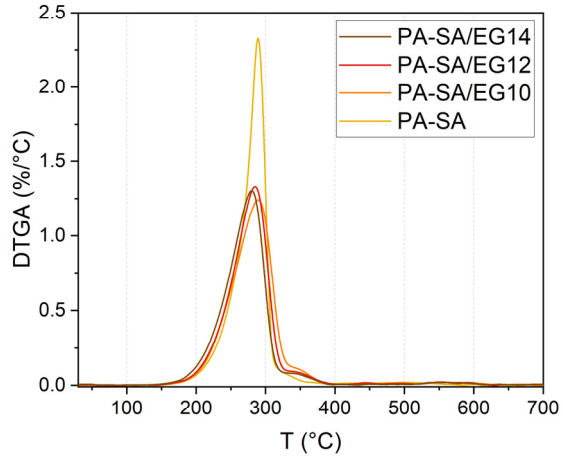

(**b**)

Figure S2. TGA curves in air atmosphere: (**a**) Residual mass; (**b**) Derivative of mass loss (DTGA).

Table S1. Selected results of TGA and DTGA analyses in air.

Sample	T_{onset} [°C]	$T_{5\%}$ [°C]	T_{peak} [°C]	m_{200} [wt.%]	m_{500} [wt.%]	m_{600} [wt.%]	m_{700} [wt.%]
PA-SA	165.5	226.7	289.2	98.6	1.0	0.0	0.0
PA-SA/EG10	161.0	224.2	289.3	98.6	9.9	8.3	7.6
PA-SA/EG12	158.0	222.0	285.0	98.4	11.9	10.4	9.9
PA-SA/EG14	151.8	214.5	279.8	97.4	13.3	11.8	11.1
EG	-	-	-	99.8	98.1	98.3	96.0

PCM oxidation between 325 °C and 400 °C, which does not occur in nitrogen atmosphere (Figure 7 and Table 3), is observable, accompanied to less pronounced mass loss in this temperature range.

3. Differential scanning calorimetry (DSC)

In Table S2 the transition enthalpies and temperatures (peak and interval) at the different scanning rates are reported (Figure 8).

Table S2. Results of DSC tests at 0.1 °C/min, 1 °C/min and 10 °C/min of neat PA-SA.

Scanning rate [°C/min]	T_m [°C]	ΔT_m [°C]	ΔH_m [J/g]	T_c [°C]	ΔT_c [°C]	ΔH_c [J/g]
0.1	53.3	51 - 54	191.5	51.3	52 - 49	191.3
1	54.6	50 - 56	195.4	49.5	52 - 43	193.3
10	59.6	50 - 68	198.3	44.3	50 - 34	195.6

T_m: melting temperature peak; ΔT_m: melting temperature interval; ΔH_m: melting enthalpy; T_c: crystallization temperature; ΔT_c: crystallization temperature interval; ΔH_c: crystallization enthalpy.

Similar values of enthalpy changing the scanning rate are noticeable, while increasing it, a shift toward higher melting temperatures and lower crystallization temperatures occurs, accompanied to a broadening of the transition temperature interval due to thermal inertia effects.

4. Test in climatic chamber

In Figures S3–S6 magnifications of the temperature profiles obtained from the tests into climatic chamber are reported and in Tables S3–S6 for each subsequent day (superscript number) the time to reach 57 °C during heating (t_{57}) from the start of the test, the maximum daily peak temperature (T_{max}), the time to reach 53 °C in cooling (t_{53}) and the minimum temperature (T_{min}) are listed.

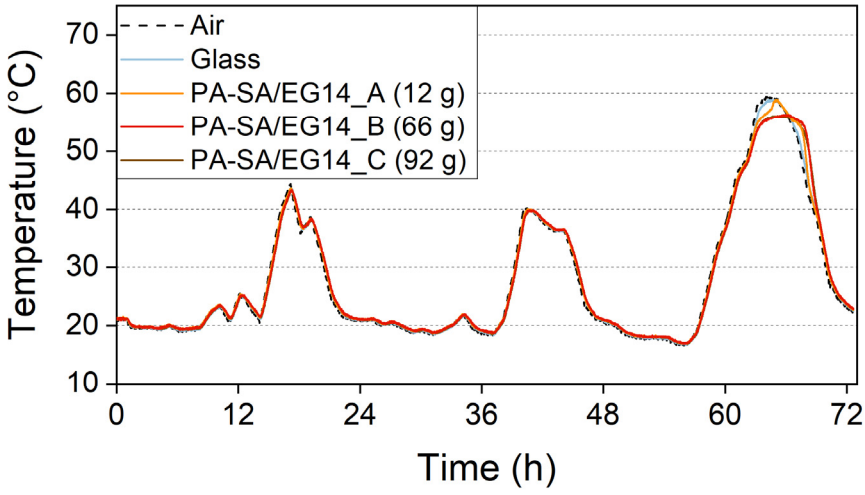

Figure S3. Climatic chamber simulations with PA-SA/EG14 bricks during the three coldest days in Verona: 18 August 2022 – 19 August 2022 – 20 August 2022.

Table S3. Characteristic times and temperatures in the reproduction of the three coldest days in Verona: 18 August 2022 – 19 August 2022 – 20 August 2022.

Sample	t_{57}^1 [h]	T_{max}^1 [°C]	t_{53}^1 [h]	T_{min}^1 [°C]	t_{57}^2 [h]	T_{max}^2 [°C]	t_{53}^2 [h]	T_{min}^2 [°C]	t_{57}^3 [h]	T_{max}^3 [°C]	t_{53}^3 [h]	T_{min}^3 [°C]
Air	-	44.3	-	19.0	-	40.5	-	17.7	63.5	59.4	68.0	16.5
Glass	-	43.6	-	19.2	-	40.0	-	17.8	63.8	58.9	68.1	16.8
PA-SA/EG14_A	-	43.6	-	19.3	-	40.1	-	18.7	65.4	58.9	68.7	16.9
PA-SA/EG14_B	-	43.3	-	19.3	-	40.0	-	18.7	-	56.4	68.9	16.9
PA-SA/EG14_C	-	43.2	-	19.3	-	39.8	-	18.7	-	56.4	68.8	16.8

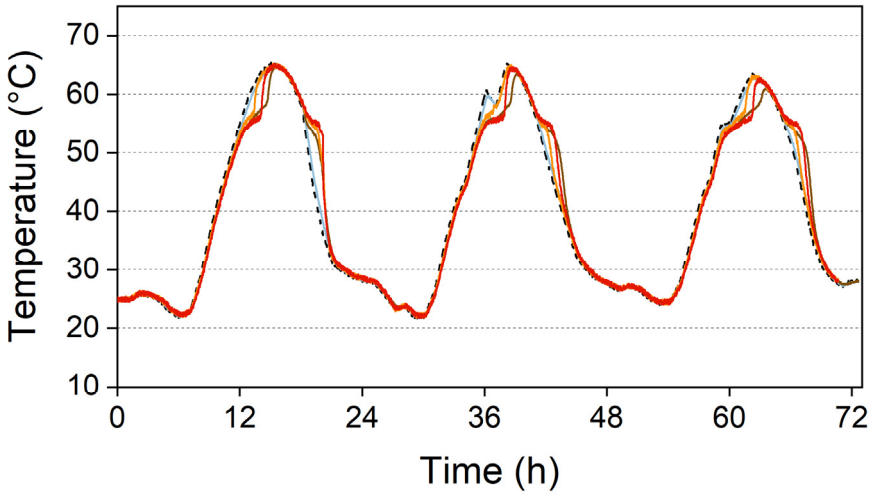

Figure S4. Climatic chamber simulations with PA-SA/EG14 bricks during the three hottest days in Verona: 22 July 2022 – 23 July 2022 – 24 July 2022.

Table S4. Characteristic times and temperatures in the reproduction of the three hottest days in Verona: 22 July 2022 – 23 July 2022 – 24 July 2022.

Sample	t_{57}^{1} [h]	T_{max}^{1} [°C]	t_{53}^{1} [h]	T_{min}^{1} [°C]	t_{57}^{2} [h]	T_{max}^{2} [°C]	t_{53}^{2} [h]	T_{min}^{2} [°C]	t_{57}^{3} [h]	T_{max}^{3} [°C]	t_{53}^{3} [h]	T_{min}^{3} [°C]
Air	12.4	65.5	18.5	21.0	35.6	65.4	41.5	21.6	60.5	63.7	65.7	23.9
Glass	12.6	65.2	18.6	21.9	35.8	64.9	41.6	21.8	60.7	63.1	65.9	24.0
PA-SA/EG14_A	13.4	65.3	19.7	21.9	36.6	65.0	42.2	21.8	61.5	63.2	66.5	24.0
PA-SA/EG14_B	14.1	65.3	19.9	21.9	37.8	64.7	42.8	21.9	62.0	62.8	66.7	24.1
PA-SA/EG14_C	13.8	64.7	19.6	22.1	38.0	63.5	42.9	21.9	62.3	61.0	67.1	24.3

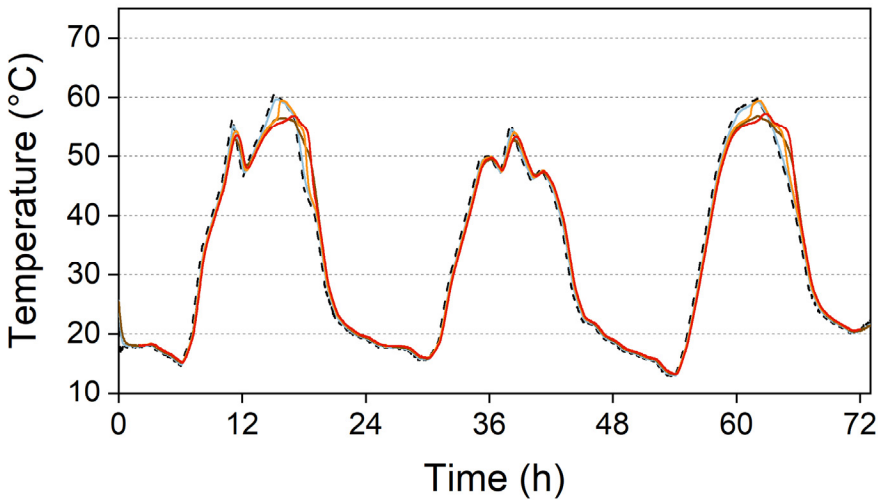

Figure S5. Climatic chamber simulations with PA-SA/EG14 bricks during the three coldest days in Gela: 08 June 2022 – 09 June 2022 – 10 June 2022.

Table S5. Characteristic times and temperatures in the reproduction of the three coldest days in Gela: 08 June 2022 – 09 June 2022 – 10 June 2022.

Sample	t_{57}^{1} [h]	T_{max}^{1} [°C]	t_{53}^{1} [h]	T_{min}^{1} [°C]	t_{57}^{2} [h]	T_{max}^{2} [°C]	t_{53}^{2} [h]	T_{min}^{2} [°C]	t_{57}^{3} [h]	T_{max}^{3} [°C]	t_{53}^{3} [h]	T_{min}^{3} [°C]
Air	13.5	60.3	16.4	14.7	-	55.4	37.6	15.6	59.0	59.8	63.8	13.0
Glass	13.7	59.6	16.6	15.1	-	54.5	37.7	15.9	59.2	59.7	64.0	13.2
PA-SA/EG14_A	14.5	59.5	17.1	15.1	-	54.0	37.8	15.9	60.1	59.8	64.6	13.2
PA-SA/EG14_B	-	56.9	17.5	15.2	-	53.3	37.8	15.9	61.5	59.6	65.1	13.2
PA-SA/EG14_C	-	56.5	17.8	15.1	-	52.6	-	15.9	-	56.9	65.5	13.2

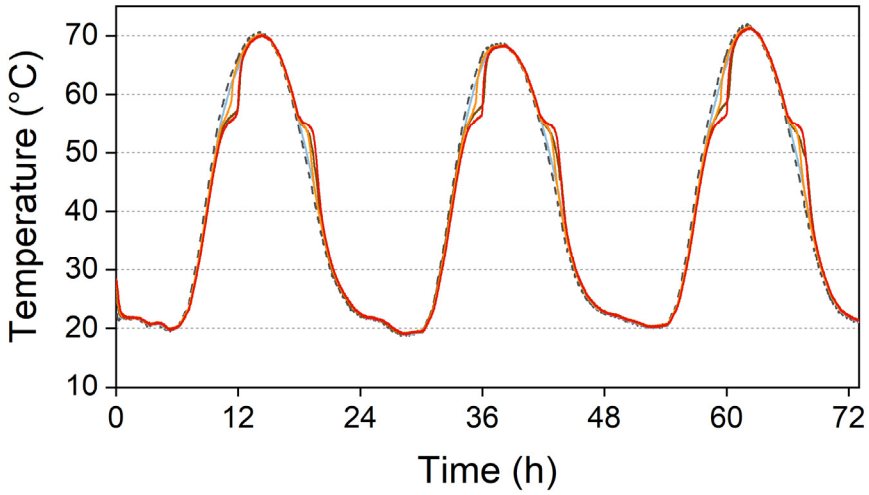

Figure S6. Climatic chamber simulations with PA-SA/EG14 bricks during the three hottest days in Gela: 26 June 2022 – 27 June 2022 – 28 June 2022.

Table S6. Characteristic times and temperatures in the reproduction of the three hottest days in Gela: 26 June 2022 – 27 June 2022 – 28 June 2022.

Sample	t_{57}^{1} [h]	T_{max}^{1} [°C]	t_{53}^{1} [h]	T_{min}^{1} [°C]	t_{57}^{2} [h]	T_{max}^{2} [°C]	t_{53}^{2} [h]	T_{min}^{2} [°C]	t_{57}^{3} [h]	T_{max}^{3} [°C]	t_{53}^{3} [h]	T_{min}^{3} [°C]
Air	10.3	70.7	18.1	19.5	34.3	68.7	42.0	18.8	58.4	72.0	66.2	20.0
Glass	10.5	70.2	18.3	19.8	34.6	68.4	42.1	19.0	58.6	71.5	66.4	20.2
PA-SA/EG14_A	11.0	70.2	18.9	19.8	35.1	68.5	42.8	19.1	59.1	71.5	67.0	20.2
PA-SA/EG14_B	11.8	70.2	19.2	19.8	35.9	68.5	43.1	19.1	60.0	71.5	67.3	20.2
PA-SA/EG14_C	11.8	70.2	19.0	19.8	35.4	68.4	42.8	19.2	59.2	71.4	67.0	20.2

5. Thermal management systems properties comparison

In Table S7 the main properties of the three studied composite materials are summarized.

Table S7. Properties comparison of thermal management systems.

TMS bricks	ρ [g/cm³]	*SD* [kg/m²]	c_{p30} [J/(g K)]	λ_{30} [W/(m K)]	T_m [°C]	T_c [°C]	ΔH_m [J/g]	*TMA* [MJ/m²]
PA-SA/EG10	0.92	18.4	1.97	4.6	54.5	50.2	181	3.4
PA-SA/EG12	0.93	18.6	1.93	7.5	53.4	50.9	176	3.3
PA-SA/EG14	0.94	18.8	1.93	8.3	53.6	50.7	169	3.2

ρ = density, *SD* = surface density of a panel of thickness 2 cm, c_{p30} = the specific heat capacity at 30 °C, λ_{30} = thermal conductivity at 30 °C, T_m = melting temperature, T_c = crystallization temperature, ΔH_m = melting enthalpy, *TMA* = thermal management ability of a system having thickness 2 cm normalized to the surface, which corresponds to the heat that the device is able to remove from the PV cell.